Macedonian Journal of Chemistry and Chemical Engineering, Vol. **42**, No. 2, pp. 249–262 (2023)

MJCCA9 – 889

ISSN 1857-5552
e-ISSN 1857-5625

Received: October 10, 2023
Accepted: October 30, 2023

DOI: 10.20450/mjcce.2023.2775
Original scientific paper

SINGLE-STEP, ELECTROPHORETICALLY DEPOSITED HYDROXYAPATITE/POLY(VINYL ALCOHOL)/CHITOSAN/GENTAMICIN COATING FOR BIOMEDICAL APPLICATIONS

Nevena Jaćimović[1], Marija Djošić[2], Ana Janković[1*], Svetlana Grujić[1], Ivana Matić Bujagić[3], Jovica Stojanović[2], Maja Vukašinović-Sekulić[1],Vesna Kojić[4], Vesna Mišković-Stanković[5]

[1]*Faculty of Technology and Metallurgy, University of Belgrade, Karnegijeva 4, 11000 Belgrade, Serbia*
[2]*Institute for Technology of Nuclear and Other Mineral Raw Materials, Bulevar Franš d'Eperea 86, Belgrade, Serbia*
[3]*Academy of Applied Technical Studies Belgrade, Katarine Ambrozić 3, 11000 Belgrade, Serbia*
[4]*Oncology Institute of Vojvodina, University of Novi Sad, Put Dr Goldmana 4, 21204 Sremska Kamenica, Serbia*
[5]*Faculty of Ecology and Environmental Protection, University Union – Nikola Tesla, Cara Dušana 62-64, 11158 Belgrade, Serbia*

ajankovic@tmf.bg.ac.rs

Biocomposite hydroxyapatite/poly(vinyl alcohol)/chitosan/gentamicin coatings were fabricated on titanium by an electrophoretic deposition process (EPD) from an aqueous suspension using the constant voltage method. Characterization of the deposited coatings was performed by scanning electron microscopy with field emission (FE–SEM), Fourier transform infrared spectroscopy (FT-IR), and X-ray diffraction (XRD) after immersion in simulated body fluid (SBF) at 37 °C. The concentration of the released gentamicin was determined using high-performance liquid chromatography (HPLC) coupled with a mass spectrometer (MS). The release profile confirmed an initial "burst-release effect" with ~ 30 % of the gentamicin released in the first 48 h, which could be of assistance in the prevention of biofilm formation. Antibacterial activity was proven by the agar diffusion method on *Staphylococcus aureus* TL and *Escherichia coli* ATCC 25922 bacterial strains. Cytotoxicity was tested by the dye exclusion test (DET) on MRC-5 and L929 fibroblast cell lines, with both coatings expressing nontoxicity. The results showed the high applicability potential of a poly(vinyl alcohol)-based biocomposite coating for medical purposes.

Keywords: antibacterial; gentamicin release; poly(vinyl alcohol); chitosan; electrophoretic deposition

ЕЛЕКТРОФОРЕТСКИ ВО ЕДЕН ЧЕКОР НАНЕСЕН ПРЕМАЗ ОД ХИДРОКСИАПАТИТ/ПОЛИ(ВИНИЛ АЛКОХОЛ)/ХИТОЗИН/ГЕНТАМИЦИН ЗА БИОМЕДИЦИНСКИ ЦЕЛИ

Биокомпозитни премази од хидроапатит/поли(винил алкохол)/хитозин/гентамицин на титаниум беа произведени со процес на електронанесување (EPD) од водна суспензија, со примена на метод на константен напон. Карактеризацијата на нанесените премази беше извршена со скенирачка електронска микроскопија со емисија на поле (FE–SEM), Фуриеова трансформна инфрацрвена спектроскопија (FT-IR) и рендгенска дифракција (XRD) откако беа потопени во симулиран телесен флуид на 37 °C. Концентрацијата на ослободениот гентамицин беше одредена со примена на високоефикасна течна хроматографија (HPLC) спрегната со масен спектрометар (MS). Профилот на ослободувањето го потврди „ефектот на експлозивно ослободување", при што 30 % од гентамицинот се ослободува во првите 48 h, што помага во спречување на образување биофилм. Антибактериската активност беше потврдена со методот на агарна дифузија на бактериските соеви *Staphylococcus aureus* TL и *Escherichia coli* ATCC 25922. Цитотоксичноста

беше тестирана со тестот за исклучување на бојата (DET) на клеточните линии на фибробластите MRC-5 и L929, при што и двата премаза покажаа дека не се токсични. Резултатите покажаа висок потенцијал за применливост на биокомпозитниот премаз базиран на поли(винил алкохол) за медицински цели.

Клучни зборови: антибактериски; ослободување на гентамицин; поли(винил алкохол); хитозин; електрофоретско нанесување

1. INTRODUCTION

Synthetic biomaterials have attracted much attention from the scientific community and health institutions due to their great possibilities for implementation in various branches of regenerative medicine.[1] The most widely researched biomaterials are bioceramic composites for applications in dentistry and orthopedics.[2,3] Titanium (Ti) is still the most commonly used metallic material in reconstruction surgery due to its good mechanical properties and corrosion resistance.[4,5] To improve biocompatibility and bioactivity and prevent bacterial biofilm formation, surface modification of titanium could be performed.[6–8] Coating by hydroxyapatite ($Ca_{10}(PO_4)_6(OH)_2$) (HAP) is very often a good choice due to its similarity to the mineral part of natural bone tissue.[9,10] As HAP is such a brittle material,[11] synthetic and/or natural polymers are often used in producing HAP-based composites to provide good adhesion and improve the mechanical properties of the coatings.[11–14] The natural polymer chitosan (CS) is a low-toxicity, biocompatible, and biodegradable material. It has a wide range of applications, e.g., in dental therapy, drug and gene-delivery systems, wound healing, treating skin after severe burns, etc.[15–17] Poly(vinyl alcohol) (PVA) is a synthetic, non-toxic, chemically stable, biocompatible, water-soluble, biodegradable polymer. It has found applications in various pharmaceutical and biomedical areas, e.g., artificial cartilage, tissue engineering, drug carriers, and wound dressing.[18-22] PVA is used to immobilize chitosan, reducing the crystallinity of the CS network and thus enabling strong interactions among functional groups.[23,24] Chitosan and PVA are known to possess high film-forming ability.[25,26] A combination of PVA and CS can improve coatings´ adhesion to metal substrates and mechanical characteristics.

Surgical site infections caused by microorganism colonization and contamination represent more than 30% of in-hospital infections, having a huge impact on morbidity and mortality in patients. With the aim of successfully preventing and treating infections, the fundamental issue is to choose the appropriate type of antibiotic. The antibiotic must be sensitive towards a broad antibacterial spectrum (both Gram-negative and Gram-positive bacteria) and have a low percentage of resistant species.[27] The use of antibiotic prophylaxis can potentially reduce post-surgical complications,[28] but prolonged antibiotic therapy can cause antimicrobial resistance across bacterial, fungal, protozoal, and viral infections. Nowadays, the prevention of post-surgery conditions can be provided by applying sufficient doses of antibiotics at the implantation site during surgical procedures, preventing biofilm formation on the surrounding tissue.[29] There are two different approaches when applying local antibiotic therapy, e.g., the application of bioceramic and/or bioactive glasses or the application of antibiotic-loaded polymers. Antibiotic-loaded polymethyl methacrylate (PMMA) beads or bead chains can be applied directly *in situ* as local antibiotic delivery to prevent biofilm formation.[30] Although good results are achieved this way, PMMA beads are intended for temporary use, needing second-stage surgery to remove them and a reconstructive procedure to fill the void.[31] On the other hand, applying bioceramics and bioactive glasses allows single-step surgery, omitting the need for additional surgical procedures.[31] The injection of antibiotics in bioceramics can improve the implant's ability to prevent biofilm formation. A significant number of post-surgery orthopedic or fracture fixation infections are caused by *Staphylococcus aureus*, Gram-positive bacteria.[32,33] Very often, the antibiotic of choice is gentamicin (Gent),[34–38] a water-soluble, wide-spectrum, aminoglycoside antibiotic sensitive to both Gram-negative and Gram-positive bacteria.[27,29,33,39,40] Due to its numerous advantages (e.g., uniform composition and thickness of the deposited coatings, the possibility of deposition on substrates of complex geometries found in orthopedics, low degree of environmental pollution, and room temperature processing, which is crucial for deposition of bioceramic coatings containing thermolabile antibacterial agents)[41] electrophoretic deposition (EPD) was chosen for the production of biocomposite coatings loaded with Gent.[41–45]

Electrophoretic deposition of composite coatings containing chitosan and gentamicin (along with methyl-cellulose,[46] gelatin and bioactive glass,[47] gelatin, silica-gentamicin and bioactive glass,[48] hydroxyapatite[49], etc.) has been reported in the literature. Gentamicin could be introduced into the composite coatings by pre-loading[48,50] or in a single-step process.[46,47,49]

In this research, we represent novel results dealing with biocompatibility and antibacterial properties, as well as bioactivity and mathematical modeling of the gentamicin release from a composite coating of unique composition, i.e., hydroxyapatite/poly(vinyl alcohol)/chitosan/gentamicin, obtained from a four-component aqueous suspension by single-step electrophoretic deposition. The formation of organosolvent-free biocompatible composite coatings deposited from aqueous suspension is especially advantageous due to the potential applications in reconstructive surgery where local drug administration is needed.

2. EXPERIMENTAL

Materials. Hydroxyapatite powder (particles < 200 nm particle size, Sigma-Aldrich), chitosan powder (medium molecular weight, 190–310 kDa with 75–85 % deacetylation degree, Sigma-Aldrich), poly(vinyl alcohol) (medium molecular weight 89–98 kDa, 99 % hydrolyzed, Sigma-Aldrich), and aqueous gentamicin sulfate solution (concentration 50 mg/ml, Sigma-Aldrich) were used. Titanium plates, Ti, (99.7 % purity, 0.25 mm thickness, Sigma-Aldrich) were mechanically polished before EPD (grit emery paper) and ultrasonicated (15 min in acetone and 15 min in ethanol). Ti plate dimensions used for all characterization methods were 1 × 1 cm, except for the cytotoxicity assay where 0.5 × 0.5 cm Ti plates were used.

Electrophoretic deposition. EPD was performed in an aqueous suspension consisting of hydroxyapatite (1.0 wt%), chitosan (0.05 wt%), and poly(vinyl alcohol) (0.1 wt%) for HAP/PVA/CS coatings, with the addition of gentamicin sulfate (0.1 wt%) for HAP/PVA/CS/Gent coatings. The pH value was 4.23.

The CS solution was prepared by dissolving 0.05 g of CS in a 1% acetic acid solution under vigorous stirring and ultrasonication for 6 h. PVA (0.1 g) was dissolved in water by stirring and heating for 2 h at 90 °C. The PVA solution was then cooled to room temperature and added to the CS solution drop-wise under constant stirring. HAP (1.0 g) was added to the PVA/CS solution under vigorous stirring followed by ultrasonication. After complete homogenization of the HAP/PVA/CS suspension, Gent (2 ml of gentamicin sulfate in 100 ml suspension) was added. The HAP/PVA/CS/Gent suspension was refrigerated and aged for 5 days. The cathodic EPD process was performed on the titanium plate (working electrode, cathode) under constant stirring. Two platinum panels (counter electrodes, anodes) were placed parallel to the Ti plate at distances of 1.5 cm. An EV231 Electrophoresis Power Supply (Peqlab, Erlangen, Germany) was employed as a constant voltage source. Coatings were deposited at previously determined optimal deposition parameters, e.g., a constant voltage of 7 V and deposition time of 12 min. Optimal deposition parameters for the EPD process were determined in the voltage range from 5 to 8 V and for deposition times between 5 and 25 min (data not shown). The optimal parameters were determined to be 7 V and 12 min, according to the adhesion test, the coatings' mass, and surface homogeneity. After deposition at optimal conditions, the coatings were air-dried at room temperature for 24 hours. Coatings thicknesses were 3.0 ± 1.1 μm and 3.1 ± 0.9 μm for HAP/PVA/CS and HAP/ PVA/CS/Gent coatings, respectively.[51]

Characterization. Scanning electron microscopy with field emission (FE-SEM) was employed to examine the surface morphology of HAP/PVA/CS and HAP/PVA/CS/Gent coatings deposited on the Ti substrate before and after immersion in simulated body fluid (SBF). A Mira 3 XMU FEG-SEM (Tescan, Czech Republic) instrument, operated at a voltage of 20.0 kV with a secondary electron detector (SE), was used. The coatings were analyzed by Fourier transform infrared spectroscopy (FT-IR) in ATR mode (range from 4000 to 400 cm^{-1}) using a Nicolet iS10 FT-IR spectrometer (Thermo Scientific, Sweden) with a resolution of 4 cm^{-1}. X-ray diffraction (XRD) analysis was performed by a powder diffractometer (Philips PW 1710, Philips, the Netherlands) with Ni-filtered Cu Kα radiation (λ = 1.5418 Å). The diffraction intensity was recorded between 4 and 70° at a step of 0.05°. Composite coating adhesion strength was investigated according to ISO 2409,[52] and tests were performed in triplicate.

Gentamicin release. The experimental procedure for determining the total amount of gentamicin loaded on coated Ti plates is described in detail in our previously published papers.[42,44] In brief, the total amount of gentamicin transferred to the coating during the EPD process was determined after the complete dissolution of the

scrapped coating in acidified deionized water. As a model system, gentamicin release studies were performed during 21-day immersion in deionized water at 37 °C, and all the measurements were done in triplicate. High-performance liquid chromatography (HPLC) (Dionex UltiMate® 3000 LC system, Thermo Fisher Scientific, USA) was utilized for gentamicin component separation. The detection and quantitative analyses were done in a linear ion trap mass spectrometer (MS) (TQ XL, Thermo Fisher Scientific) with an electrospray ionizer. The HPLC was equipped with a reverse-phase column (75 mm × 4.6 mm, 3.5 μm) Zorbax Eclipse® XDB-C18 (Agilent Technologies, USA), in front of which a pre-column (12.5 mm × 4.6 mm, 5 μm) was placed. Methanol (A), deionized water (B), and 10 % acetic acid (C) comprised the mobile phase. The optimized HPLC and MS operating parameters (mobile-phase gradient, analytes' precursor ions, fragmentation reactions used for quantification, and optimal collision energies) for the determination of gentamicin compounds were published in our previous paper.[44] The gentamicin mass spectra were collected in the *m/z* range of 50–1000. As expected, the MS spectrum revealed the three most abundant ions since gentamicin is composed of three compounds: gentamicin C1a, C2, and C1. These ions were further chosen as the precursor ions for each compound. Their most sensitive transitions were selected for quantification purposes. The gentamicin concentrations presented represent sums of the three determined gentamicin compounds.

Antibacterial activity. The agar diffusion test of antibacterial activity was performed in Lennox broth medium containing 0.7 wt% of agar in the final volume. The heated medium was poured into Petri dishes forming thick layers (~4 mm) and densely inoculated with Gram-negative *Escherichia coli* ATCC 25922 and pathogenic Gram-positive *Staphylococcus aureus* TL (collection of cultures of the University of Belgrade, Faculty of Technology and Metallurgy) bacterial strain cultures not older than 18 h in concentrations 10^5–10^6 CFU/ml. The Petri dishes were left for 15 min at room temperature. HAP/PVA/CS and HAP/PVA/CS/Gent coatings (10×10 mm on Ti plates of 1 mm thickness), previously sterilized in an autoclave at 121 °C for 30 min, were then placed onto the agar surface. After overnight incubation at 37 °C, samples displayed antibacterial activity, which was subsequently evaluated by measuring the diameters of the inhibition zones.

Cytotoxicity. The cytotoxicity of HAP/PVA/CS and HAP/PVA/CS/Gent coatings was tested by dye exclusion test (DET) using two fibroblast cell lines (L929 and MRC-5). The L929 (ATCC CRL-6364) mouse-origin cell line was used along with the MRC-5 (ATCC CCL-171) human fibroblast line. As per the FDA Biological Evaluation Guidance and the recommendations given by International Standard ISO 10993-1, cytotoxicity testing of a new medical implant material was conducted on a mice fibroblast cell line L929 (ATCC CRL-6364). Human-origin fibroblast cell line MRC-5 was also tested due to its similarity to the targeted connective tissue. A standardized cell propagation protocol was used where cells were cultivated in DMEM medium supplemented with 10% fetal calf serum (FCS) and antibiotics antimycotic solution (Sigma). Cells were subcultured twice a week and trypsinized in EDTA (Serva), 0.1 wt % solution, to achieve a single-cell suspension. Flasks of 25 cm^2 (Costar) were used for cell line culturing at 37 °C, 100 % humidity, and 5 % CO_2. Cells in the exponential phase of growth were used for all the assays.

Statistical analysis. One-way analysis of variance (ANOVA) was used to evaluate the statistical significance of the cytotoxicity assay results. The differences between the samples were statistically evaluated by comparing the calculated *p*-value to the *p*-value of the null hypothesis with a significance level of 0.05. The results were considered statistically significant if the *p*-value was lower than 0.05.

3. RESULTS AND DISCUSSION

3.1. *FT-IR analysis*

FT-IR spectra of biomimetically grown HAP on the top of HAP/PVA/CS and HAP/PVA/CS/Gent coatings on Ti after immersion in SBF at 37 ºC for 7 and 14 days are represented in Figs.1a and b, respectively. The positions of detected bands are listed in Table 1. Characteristic bands confirming the presence of PO_4^{3-} groups can be detected in two regions: 450–620 cm^{-1} (O-P-O bending modes in the phosphate group) and 900-1200 cm^{-1} (P-O stretching vibrations of the phosphate group).[42–44,49] Hydroxyl groups in the HAP structure can be detected at around 630 cm^{-1} (OH^- bending) and at 3568 cm^{-1} (OH^- stretching),[43,49,53] for all of four biomimetically grown HAP coatings. The wide bands at around 3300 cm^{-1} (for HAP/PVA/CS) and 3350 cm^{-1} (for HAP/PVA/CS/Gent) can be assigned to the adsorbed water.[54–56] As reported in the literature,[57] carbonate bands can be detected at approximately 872, 879, 1415, 1455,

and 1468 cm^{-1} for all biological apatites. Natural bone consists of an organic phase (collagen) and a mineral phase (substituted hydroxyapatite). The substitution with carbonate groups occurred between hydroxyl and phosphate groups from HAP, leading to the formation of A- and B-type substituted HAP, respectively, or combined AB-type substitution.[45,54] As represented in Figure 1, the vibrational mode of the O-C-O group can be detected at around 873 cm^{-1}, while bands in the region 1400–1500 cm^{-1} can be attributed to the O-C group vibrational mode.[42] Based on the position of carbonate bands in HAP layers grown on the top of HAP/PVA/CS and HAP/PVA/CS/Gent coatings after immersion in SBF at 37 ºC for 7 and 14 days (Table 1), it can be concluded that both AB- and B-type substitution in HAP occurred.[57,58] Bands at around 1413 and 1420 cm^{-1} can be assigned to B-type substitution in HAP, along with a band positioned at 1465 cm^{-1}, known as the "signature" band for B-type substitution in a HAP structure.[43,57] On the other side, bands positioned at around 873 and 1458 cm^{-1} can be assigned to the AB-type of substitution.[43] Therefore, for our biomimetically grown layers on the top of both coatings, B-type substitution in HAP dominated over AB-type substitution. These findings corroborated well with the results of XRD analysis (Section 3.2.), where the presence of B-type carbonated HAP was detected as a separate phase. As natural bone apatites are classified as carbonate substituted,[59] it can be proposed that our coatings, with the matching composition, could be potentially used as biomaterials.

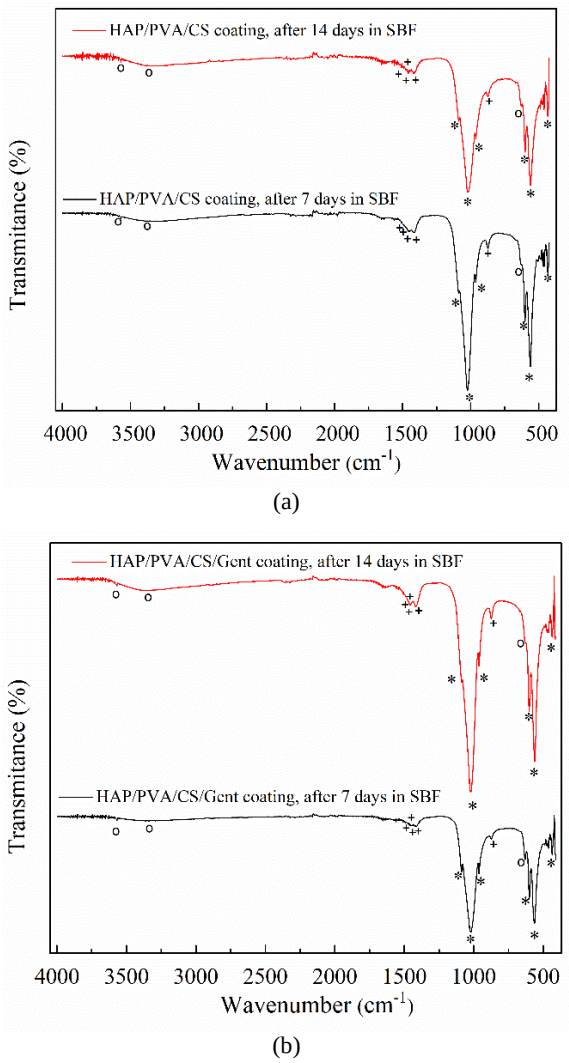

Fig. 1. FTIR spectra of (a) HAP/PVA/CS and (b) HAP/PVA/CS/Gent coatings after soaking in SBF at 37 ºC for 7 and 14 days (bands denotation: * PO_4^{3-}; + CO_3^{2-}; º OH^-)

T a b l e 1

Characteristic FTIR bands of HAP layers biomimetically grown on the top of HAP/PVA/CS and HAP/PVA/CS/Gent coatings after immersion in SBF at 37 ºC for 7 and 14 days

Coating	Group	Wavenumber, cm^{-1} [42–44,49,53,54]	
		Immersion time, days	
		7	14
HAP/PVA/CS	Vibrational modes of PO_4^{3-} group	962; 1024; 1087 468; 560; 600	962; 1020; 1087 560; 600
	Vibrational mode of OH^- group	626 3332 3568	629 3334 3568
	Vibrational mode of CO_3^{2-} group	873; 1414; 1420; 1458; 1465	873; 1413; 1420; 1458; 1465
HAP/PVA/CS/Gent	Vibrational modes of PO_4^{3-} group	961; 1022; 1087 472; 562; 600	962; 1022; 1086 472; 561; 600
	Vibrational mode of OH^- group	630 3357 3568	628 3345 3568
	Vibrational mode of CO_3^{2-} group	873; 1412; 1420; 1458; 1466	874; 1414; 1420; 1458; 1465

3.2. *X-ray diffraction*

XRD patterns for biomimetic HAP, grown on the top of HAP/PVA/CS and HAP/PVA/CS/Gent coatings after immersion in SBF at 37 ºC for 7 and 14 days, are represented in Figure 2.

Diffraction maximums corresponding to hydroxyapatite are denoted as **1** (hydroxyapatite (HAP), JCPDS 09-0432), **2** (carbonate substituted hydroxyapatite (C-HAP), JCPDS 19-0272), and **H** (HAP and C-HAP, where diffraction maximums are overlapped). Diffraction maximums corresponding to titanium substrate (#-α-Ti, JCPDS 44-1294) were also detected. For all coatings, the broadening of diffraction maximums suggested the existence of small HAP crystallites (Fig. 2). Table 2 shows *d*-spacing values for biomimetic coatings obtained on top of HAP/PVA/CS and HAP/PVA/CS/Gent coatings after immersion in SBF for 7 and 14 days. The values were calculated from the characteristic hydroxyapatite crystal planes (002), (211), (112), (300), and (202). For newly formed biomimetic coatings, *d*-spacing values remained unchanged for different soaking periods for both HAP/PVA/CS and HAP/PVA/CS/Gent coatings.

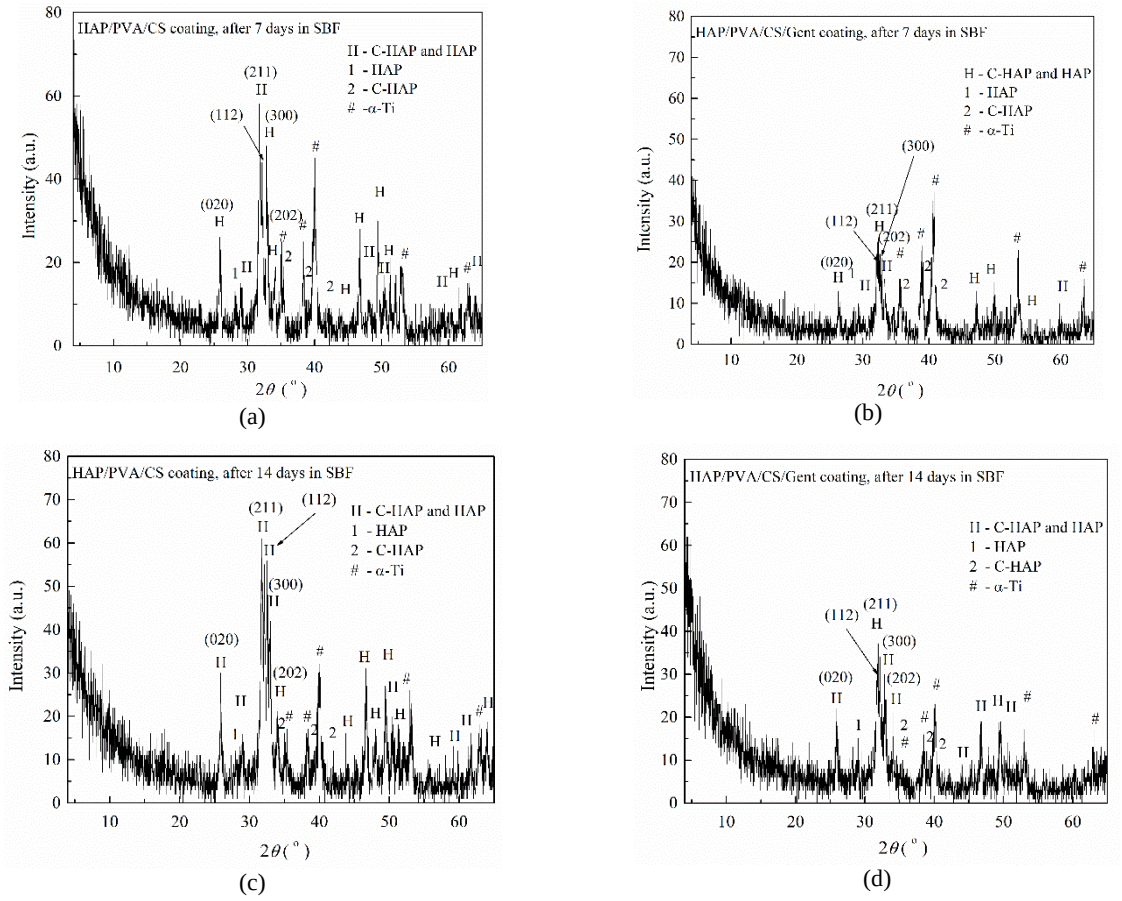

Fig. 2. XDR patterns for (a, c) HAP/PVA/CS and (b, d) HAP/PVA/CS/Gent coatings after immersion in SBF at 37 ºC for 7 and 14 days, respectively

T a b l e 2

The d-spacing values of the characteristic hydroxyapatite crystal planes

Coating	Time in SBF, days	Crystal planes				
		(002)	(211)	(112)	(300)	(202)
		d-spacing, Å				
HAP/PVA/CS	7	3.4512	2.8114	2.7811	2.7271	2.6320
HAP/PVA/CS	14	3.4514	2.8100	2.7811	2.7183	2.6300
HAP/PVA/CS/Gent	7	3.4411	2.8151	2.7805	2.7274	2.6311
HAP/PVA/CS/Gent	14	3.4487	2.8115	2.8051	2.7184	2.6300

Hydroxyapatites' characteristic crystal plane (002) was used for the calculation of unit cell parameters (*a* and *c*) and unit cell volume (*V*), as well as the crystallite domain size of biomimetically grown coatings after soaking in SBF. The results are represented in Table 3.

The growth of biomimetic HAP occurred through the parallel processes of precipitation and dissolution during exposure to the SBF solution (biomineralization process). Also, the antibiotic present in the HAP/PVA/CS/Gent coating was released during the biomineralization process. After the composite coatings were exposed to the SBF, negatively charged hydroxyl and phosphate ions from the coatings' surface attracted calcium ions from the SBF solution, leading to the formation of a supersaturated solution towards apatite, and, consequently, nucleation and growth of biomimetic HAP. Along with biomimetic HAP precipitation, its dissolution occurred, leading to an increase in Ca^{2+} and PO_4^{3-} ion concentrations on the coating surface.[60,61] The precipitation rate dominated over the dissolution rate of HAP, leading to the formation of biomimetic coatings. After drug-loaded coating (HAP/PVA/CS/Gent) exposure to SBF, the release of the antibiotic occurred simultaneously with the biomimetic HAP precipitation/dissolution. The release of an antibiotic from biodegradable systems could be described through diffusion, dissolution, and erosion mechanisms or a combination thereof.[62,63] As a consequence of all the processes mentioned above, crystallite domains for the newly grown HAP on both coatings after immersion in SBF for 7 days were very similar though slightly smaller than the crystallite domain size of as-deposited coatings, e.g., 138 Å for HAP/PVA/CS after 7-day immersion (172 Å for as-deposited HAP/PVA/CS) and 141 Å for HAP/PVA/CS/Gent after 7 days of immersion (165 Å for as-deposited HAP/PVA/CS/Gent) (Table 3).[51] On the other side, a greater difference in the crystallite domain size could be observed after 14 days of exposure to the SBF compared to the crystallite domain size of biomimetic HAP grown after 7 days of immersion in SBF. It can be assumed that the large molecule of gentamicin could suppress further growth of biomimetic HAP crystals, leading to the formation of finer crystallites in the biomimetic HAP coating formed on the top of gentamicin-loaded coating (305 Å) than in the antibiotic-free coating (421 Å). Unit cell parameters remained almost unchanged during soaking time. Based on the experimental results, both HAP/PVA/CS and HAP/PVA/CS/Gent coatings were able to induce the nucleation and growth of biomimetic HAP and, therefore, could be considered potential biomaterials for improving implant and natural bone integration. Additionally, carbonate-substituted HAP (JCPDS 19-0272), detected in all biomimetic coatings, is known to be B-type substituted ($Ca_{10}(PO_4)_3(CO_3)_3(OH)_2$).[64] Based on literature data, all carbonate substitutions in bone minerals are primarily B-type substitutions.[65] Judging on this property alone, our coatings are promising biomaterials for osseointegration.

T a b l e 3

Unit cell parameters (a and c), unit cell volume (V), and crystallite domain size of hydroxyapatite layer on the top of HAP/PVA/CS and HAP/PVA/CS/Gent coatings after immersion in SBF at 37 ºC for 7 and 14 days.

Coating	Time in SBF, days	Parameter			Crystallite domain size, Å
		a, Å	*c*, Å	*V*, Å^3	
HAP/PVA/CS	0*	9.3754*	6.8549*	521.82*	172*
	7	9.4274	6.8859	530.00	138
	14	9.4585	6.8962	534.30	421
HAP/PVA/CS/Gent	0*	9.3637*	6.8400*	519.38*	165*
	7	9.4389	6.8945	531.86	141
	14	9.4449	6.8929	532.51	305

*Cell parameters of hydroxyapatite of as-deposited HAP/PVA/CS and HAP/PVA/CS/Gent coatings[51]

3.3. *Scanning electron microscopy and adhesion properties*

Figure 3 shows FE-SEM micrographs of HAP/PVA/CS (Figs. 3a and c) and HAP/PVA/CS/Gent (Figs. 3b and d) coatings before and after immersion in SBF for 7 days at 37 °C, respectively. No significant differences in the surface morphology could be observed for both coatings before immersion in SBF (Figs. 3a and b). However, hydroxyapatites´ characteristic spherical agglomerates of different sizes, embedded into the poly-

mer matrix of PVA/CS, can be visualized, meaning that the gentamicin incorporation (Fig. 3b) did not affect the coatings' morphology. SEM micrographs of HAP/PVA/CS and HAP/PVA/CS/Gent coatings after immersion in SBF are shown in Figures 3c and d, respectively. Compared to the coatings before immersion, a change in the surface morphology can be observed after only 7 days of exposure to SBF, suggesting the formation of a new biomimetic layer with needle-like shaped HAP agglomerates. Noticeable differences between the topography of newly formed HAP on the top of HAP/PVA/CS/Gent and HAP/PVA/CS coatings could be attributed to the presence of gentamicin. It is known that the release of antibiotics from a polymer matrix is governed by diffusion, dissolution, and erosion or by a combination of these three processes,[62] leading to coatings´ topography change. FE-SEM, along with XRD and FTIR results, confirmed the bioactivity of both HAP/PVA/CS and HAP/PVA/CS/Gent composite coatings after immersion in SBF through the coatings' ability to induce the growth of a new layer, facilitating bonding between implants and natural bone.

Figure 4 represents the test of the adhesion between Ti substrate and HAP/PVA/CS (Fig.4a) and HAP/PVA/CS/Gent (Fig. 4b) coatings, performed according to ISO 2409 standard (six-step classification). The adhesion test results showed the appearance of small detachments of the coatings at the intersections of the cuts (less than 5 % of the coatings' surface). These can be classified as "1", according to the ISO 2409 standard. These results suggest good adhesion properties for both composite coatings.

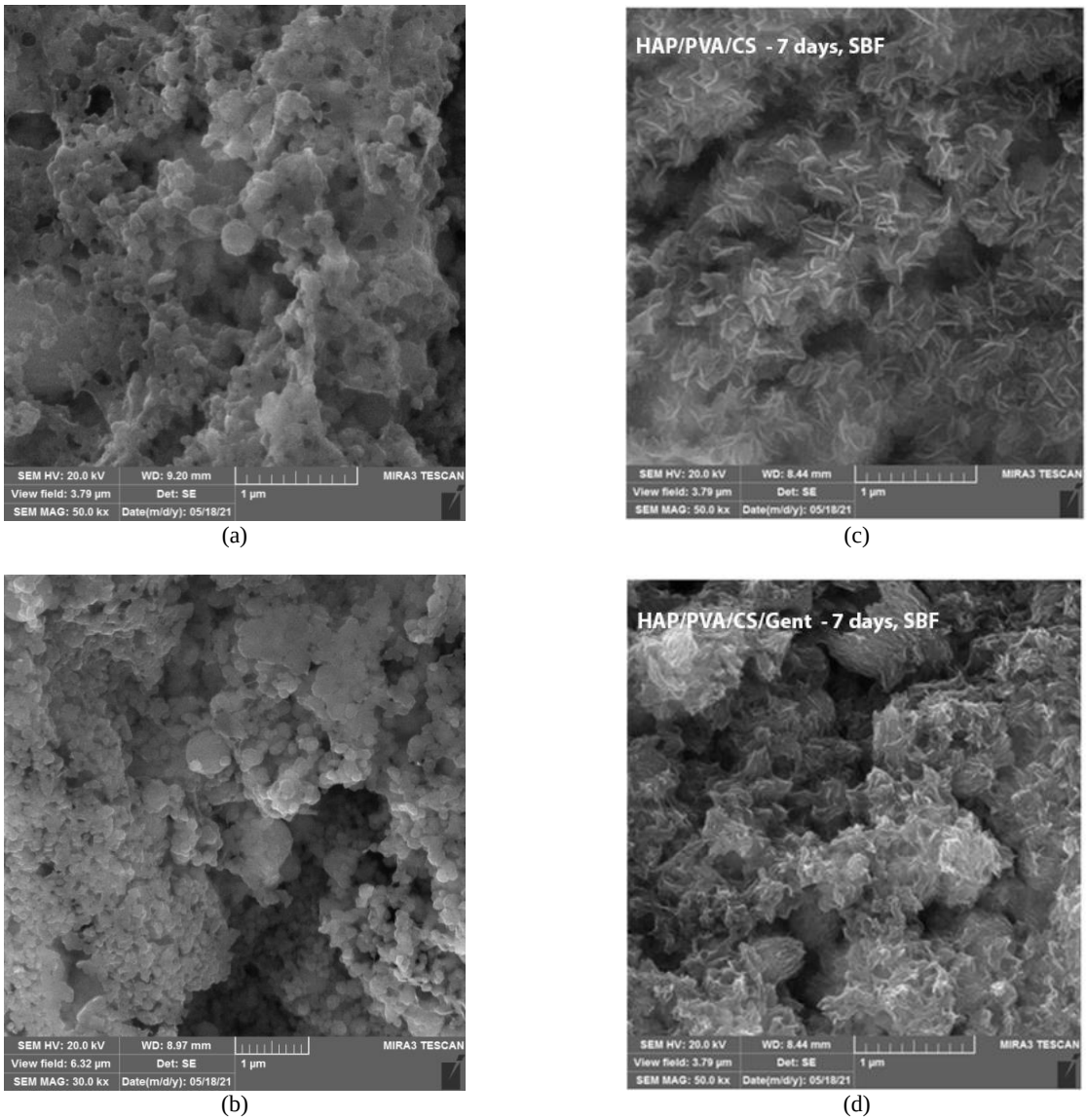

Fig. 3. SEM microphotographs of HAP/PVA/CS and HAP/PVA/CS/Gent coatings before (a, b) and after (c, d) immersion in SBF at 37°C for 7 days, respectively

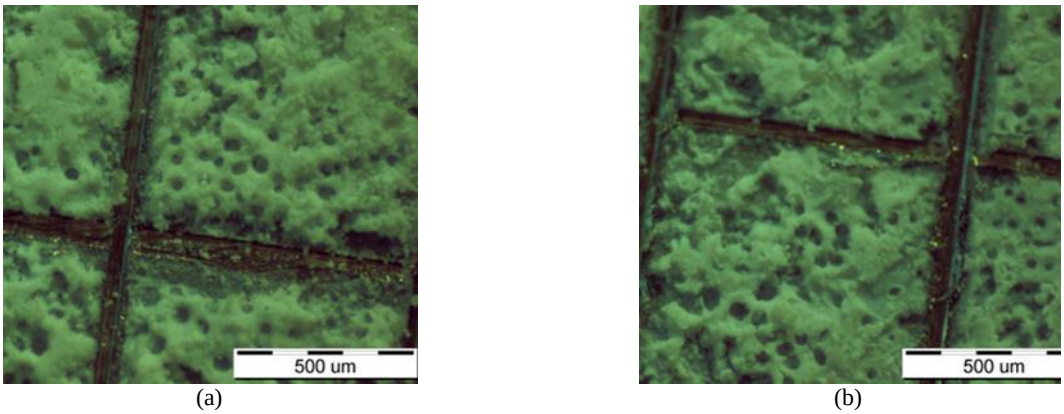

(a) (b)

Fig. 4. Test of adhesion between titanium substrate and composite coatings (a) HAP/PVA/CS and (b) HAP/PVA/CS/Gent.

3.4. *Gentamicin release*

Gentamicin release from the deposited HAP/PVA/CS/Gent coating was investigated during immersion in deionized water for 21 days (Fig. 5). The initial burst-release reaching ~30% observed in the first 48 h could be of importance in the prevention of biofilm formation by bacterial cell adhesion. After 21 days, the percentage of gentamicin released from the HAP/PVA/CS/Gent coating remained at approximately the same level.

The experimental data were fitted with early time approximation (ETA) kinetic models in order to investigate the main diffusion mechanism and determine the diffusion coefficient of gentamicin.

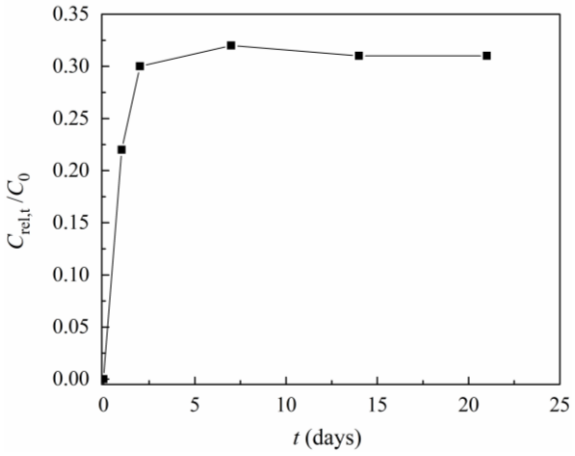

Fig. 5. Gentamicin release from HAP/PVA/CS/Gent coating in deionized water at 37 °C for 21 days

ETA assumes a linear correlation between the released amount of active substance and the square root of time. According to Ritger and Peppas[66], this model can be used for one-dimensional release from thin films, and it is utilized to calculate the diffusion coefficient of gentamicin at the time of its release from the HAP/PVA/CS/Gent coating (Equation 1):

$$\frac{C_{\mathrm{rel,t}}}{C_0} = 4 \times \sqrt{\frac{Dt}{\pi\delta^2}} \qquad (1)$$

The parameters in Equation (1) are as follows: $C_{\mathrm{rel,t}}$ is the concentration of gentamicin released at the time t; C_0 is the total initial concentration of gentamicin in the deposited coating; D is the diffusion coefficient of gentamicin; and δ is the thickness of the coating. The ETA model can be used as a Fickian diffusion model for release from thin composite films only for the initial release period. The ETA model applied to the release profile of HAP/PVA/CS/Gent coating is represented in Figure 6. The diffusion coefficient, D, of gentamicin was calculated to be $9.6 \cdot 10^{-10}$ cm^2 s^{-1}. A steady release of gentamicin from the coating could be beneficial for the intended purpose of a biocomposite in orthopedic implants because the risk of infection is the highest post-operation. This system allows targeted drug delivery with an initial release burst, thus preventing initial bacterial infection and biofilm formation at the implantation site.

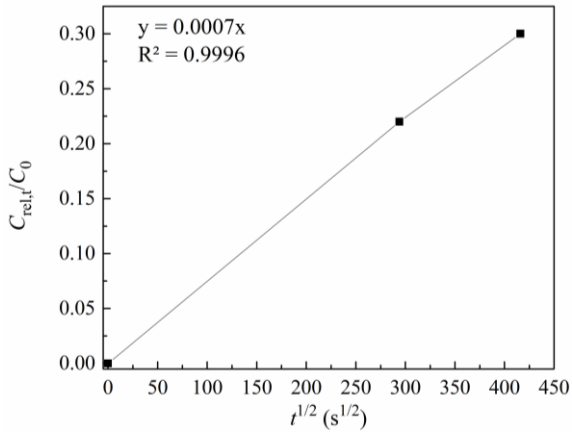

Fig. 6. Early-time approximation of gentamicin release from HAP/PVA/CS/Gent coating

3.5. *Antibacterial activity*

The antibacterial activity of HAP/PVA/CS and HAP/PVA/CS/Gent coatings against *Escherichia coli* ATCC 25922 and *Staphylococcus aureus* TL bacterial strains was examined by the agar diffusion method. The results are shown in Figure 7. Control samples of HAP/PVA/CS coatings did not show any antibacterial activity, while the HAP/PVA/CS/Gent coating was active against bacteria. In the case of *E. coli* (Fig. 7a), lighter (maximum bacterial susceptibility 19 mm in diameter) and darker (moderate bacterial susceptibility 29 mm in diameter) circular inhibition zones were observed. Against *Staphylococcus aureus* (Fig. 7b), darker (measured dimensions: width 37 mm, length 42 mm) and lighter inhibition (measured dimensions: width 32 mm, length 40 mm) zones, ellipsoidal in shape, were also noticed. According to the dimensions of the inhibition zones measured against both bacterial strains, strong activity of the selected antibacterial agent Gent could be verified against *E. coli* ATCC 25922 and *Staphylococcus aureus* TL, with stronger activity against *Staphylococcus aureus* TL. Gent is a prototype aminoglycoside antibiotic. Its mechanism of action is inhibition of protein synthesis in bacteria. Aminoglycosides, in general, and gentamicin, in particular, bind irreversibly to specific bacterial 30S protein subunits and 16S rRNA, thus preventing the formation of mRNA initiation complexes.[49] The results are in compliance with the literature data since gentamicin is generally very active against some staphylococcus and streptococcus, which explains its strong antibacterial activity against *Staphylococcus aureus* TL.[67] Although meticulously assessed, agar diffusion analysis provided more of a qualitative measure of HAP/PVA/CS/Gent coating antibacterial activity. However, these results were in excellent compliance with the quantitative monitoring of changes in the viable number of bacterial cells in suspension that we had already published for the system.[51] The antibacterial effect of HAP/PVA/CS/Gent was very prominent against *E.coli* since the bacteria cell count of 10^6 CFU ml^{-1} decreased to 10^3 CFU ml^{-1} in just 15 min of inoculation[51]. After 1h of incubation, no bacterial colonies were visualized on the plates. The same conclusion was verified for the wide inhibition zone of *E.coli* (Fig. 7a). In the case of antibiotic-loaded coating, HAP/PVA/CS/Gent, *S.aureus* viable cells were completely diminished immediately after inoculation, i.e., bacterial cell count dropped from the initial 10^6 CFU ml^{-1} to zero[51] for this Gram(+) bacterial strain. Indeed, the wide, light inhibition zone in Fig 7b confirms the calculated values. Therefore, the HAP/PVA/CS/Gent coating material could be classified as bactericidal[68] due to the effective and immediate reduction of both bacteria.

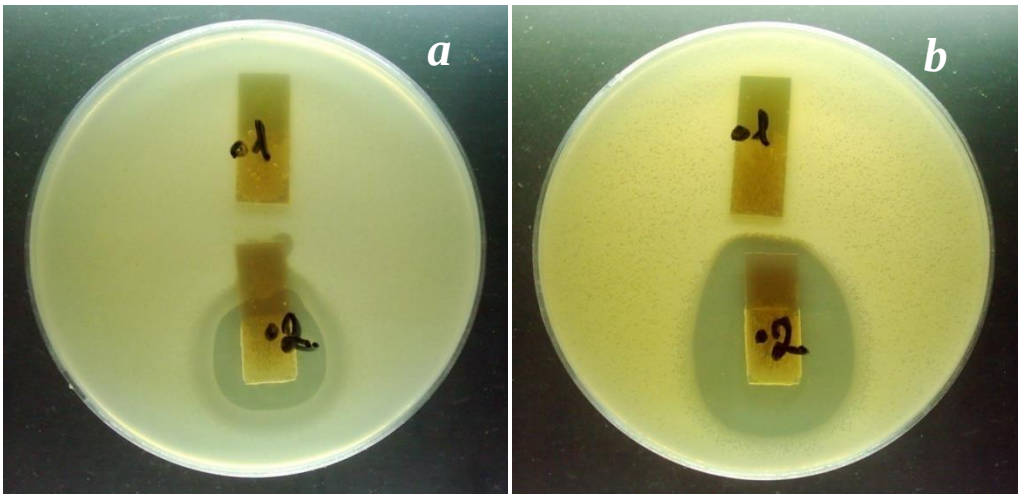

Fig. 7. Antibacterial activity of HAP/PVA/CS (control plate, 1) and HAP/PVA/CS/Gent (2) coatings against bacterial strain *E. coli* (a) and *Staphylococcus aureus* (b)

3.6. *Cytotoxicity*

The bar chart in Figure 8 depicts the results of the trypan blue DET assay for HAP/PVA/CS and HAP/PVA/CS/Gent coatings, performed on two fibroblast cell lines, human MRC-5 and mouse L929, to estimate cell viability in the presence of the material.

The Trypan blue exclusion test of cell viability is based on cell staining after mixing with the

dye. Damaged cells uptake the dye, while undamaged cells remain unstained. The evaluation of cell growth (% cell viability) was expressed as a percent of control and further estimated based on the ratio of stained and unstained cells. The HAP/PVA/CS coating slightly provoked the inhibition of growth in MRC-5 (94.2 %) and L929 (89.1 %). After the gentamicin introduction, the cell growth appeared to increase for both MRC-5 (96.9 %) and L929 (92.1 %) cell lines. The surface granulation of the HAP/PVA/CS/Gent composite coating seemed to stimulate the proliferation of both cell lines regardless of their origin.

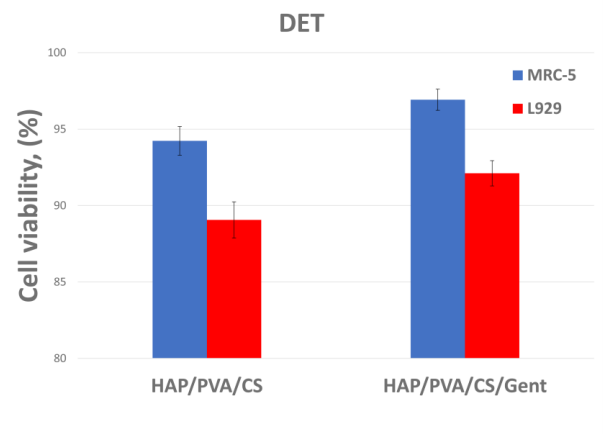

Fig. 8. Viability of MRC-5 and L929 cells (expressed as a percent of control) when exposed to HAP/PVA/CS and HAP/PVA/CS/Gent coatings. *$p < 0.05$ for the respective cell lines

4. CONCLUSION

Biocomposite poly(vinyl alcohol)-based HAP/PVA/CS and HAP/PVA/CS/Gent coatings on Ti substrates were successfully obtained by electrophoretic deposition (EPD). Homogeneous coatings of uniform thickness were assembled at a constant deposition voltage of 7 V for 12 min. The bioactivity of both HAP/PVA/CS and HAP/PVA /CS/Gent coatings after immersion in simulated body fluid (SBF) at 37 °C, i.e., the growth of a new phase of hydroxyapatite, was proven by FE-SEM, FT-IR and XRD analysis. In addition, XRD and FT-IR spectra confirmed the presence of characteristic carbonate bands and AB-type substitution in HAP structure, as well as B-type substitution. Both HAP/PVA/CS and HAP/PVA/CS/Gent coatings proved non-cytotoxic against two fibroblast cell lines – human MRC-5 and mouse L929.

Only the HAP/PVA/CS/Gent coating exhibited antibacterial activity against *Escherichia coli* ATCC 25922 and *Staphylococcus aureus* TL bacterial strains. The gentamicin release study indicated a "burst" release effect in the first 48 h, with ~ 30 % of total gentamicin released from the HAP/PVA/CS/Gent coating, which is beneficial for the blockage of biofilm formation, followed by slow and steady release in the later time period. Using the Fickian diffusion model and early time approximation, the value of diffusion coefficient, *D*, of gentamicin through the HAP/PVA/CS/Gent coating was calculated to be $9.6 \cdot 10^{-10}$ cm^2 s^{-1}.

All the above indicates good potential for the implementation of bioceramic HAP/PVA/CS/ Gent coatings on titanium implants in orthopedic and dental practice.

Acknowledgment: This research is supported by the Ministry of Science, Technological Development and Innovation, Republic of Serbia (Contract No. 451-03-47/2023-01/200287, 451-03-47/2023-01/200023, and 337-00-110/2023-05/13), and by University Union - "Nikola Tesla", Belgrade, Serbia. This research was funded by the European Union's Horizon 2020 research and innovation program under grant agreement No. 952033.

REFERENCES

(1) Brokesh, A. M.; Gaharwar, A. K., Inorganic biomaterials for regenerative medicine. *ACS Appl. Mater. Interfaces* **2020**, *12* (5), 5319–5344. https://doi.org/10.1021/acsami.9b17801

(2) Khan, A. S.; Syed, M. R., A review of bioceramics-based dental restorative materials. *Dent. Mater. J.* **2019**, *38* (2), 163–176. https://doi.org/10.4012/dmj.2018-039

(3) Zhang, X.; Song, G.; Qiao, H.; Lan, J.; Wang, B.; Yang, H.; Ma, L.; Wang, S.; Wang, Z.; Lin, H.; Han, S.; Kang, S.; Chang, X.; Huang, Y., Novel ternary vancomycin/strontium doped hydroxyapatite/graphene oxide bioactive composite coatings electrodeposited on titanium substrate for orthopedic applications. *Colloids Surfaces A Physicochem. Eng. Asp.* **2020**, *603* (May), 125223. https://doi.org/10.1016/j.colsurfa.2020.125223

(4) Kaur, M.; Singh, K., Review on titanium and titanium based alloys as biomaterials for orthopaedic applications. *Mater. Sci. Eng. C* **2019**, *102* (December 2018), 844–862. https://doi.org/10.1016/j.msec.2019.04.064

(5) Eliaz, N., Corrosion of metallic biomaterials: A review. *Materials (Basel).* **2019**, *12* (3). https://doi.org/10.3390/ma12030407

(6) Quinn, J.; McFadden, R.; Chan, C. W.; Carson, L., Titanium for orthopedic applications: An overview of surface modification to improve biocompatibility and prevent bacterial biofilm formation. *iScience* **2020**, *23* (11), 101745. https://doi.org/10.1016/j.isci.2020.101745

(7) Stepanovska, J.; Matejka, R.; Rosina, J.; Bacakova, L.; Kolarova, H., Treatments for Enhancing the Biocompatibility of Titanium Implants. *Biomed. Pap.* **2020**, *164* (1), 23–33. https://doi.org/10.5507/bp.2019.062

(8) Chouirfa, H.; Bouloussa, H.; Migonney, V.; Falentin-Daudré, C., Review of titanium surface modification

techniques and coatings for antibacterial applications. *Acta Biomater.* **2019**, *83*, 37–54. https://doi.org/10.1016/j.actbio.2018.10.036

(9) Ciobanu, G.; Harja, M., Investigation on hydroxyapatite coatings formation on titanium surface. *IOP Conf. Ser. Mater. Sci. Eng.* **2018**, *444* (3). https://doi.org/10.1088/1757-899X/444/3/032007

(10) Kien, P. T.; Quan, T. N.; Tuyet Anh, L. H., Coating characteristic of hydroxyapatite on titanium substrates via hydrothermal treatment. *Coatings* **2021**, *11* (10), 1–11. https://doi.org/10.3390/COATINGS11101226

(11) Mahanty, A.; Shikha, D., Changes in the morphology, mechanical strength and biocompatibility of polymer and metal/polymer fabricated hydroxyapatite for orthopaedic implants: A review. *J. Polym. Eng.* **2022**, *42* (4), 298–322. https://doi.org/10.1515/polyeng-2021-0171

(12) Abdulghani, S.; Mitchell, G. R., Biomaterials for in situ tissue regeneration: A review. *Biomolecules* **2019**, *9* (11). https://doi.org/10.3390/biom9110750.

(13) Raut, H. K.; Das, R.; Liu, Z.; Liu, X.; Ramakrishna, S., Biocompatibility of biomaterials for tissue regeneration or replacement. *Biotechnol. J.* **2020**, *15* (12), 1–14. https://doi.org/10.1002/biot.202000160

(14) Rajabi, A.; Esmaeili, A., Preparation of three-phase nanocomposite antimicrobial scaffold BCP/Gelatin/45S5 glass with drug vancomycin and BMP-2 loading for bone regeneration. *Colloids Surfaces A Physicochem. Eng. Asp.* **2020**, *606* (August), 125508. https://doi.org/10.1016/j.colsurfa.2020.125508

(15) Jiménez-Gómez, C. P.; Cecilia, J. A., Chitosan: A natural biopolymer with a wide and varied range of applications. *Molecules* **2020**, *25* (17). https://doi.org/10.3390/molecules25173981

(16) Song, Z.; Wang, J.; Tan, S.; Gao, J.; Wang, L., Conductive biomimetic bilayer fibrous scaffold for skin regeneration. *Colloids Surfaces A Physicochem. Eng. Asp.* **2023**, *656* (PA), 130211. https://doi.org/10.1016/j.colsurfa.2022.130211

(17) Mabrouk, M.; Abd El-Wahab, R. M.; Abo-Elfadl, M. T.; Beherei, H. H.; Selim, M. M.; Ibrahim, A. M.; Das, D. B., Magnetic nanosystems substituted with zinc for enhanced antibacterial, drug delivery and cell viability behaviours. *Colloids Surfaces A Physicochem. Eng. Asp.* **2022**, *650* (July), 129629. https://doi.org/10.1016/j.colsurfa.2022.129629

(18) Massarelli, E.; Silva, D.; Pimenta, A. F. R.; Fernandes, A. I.; Mata, J. L. G.; Arm, H.; Saramago, B.; Serro, A. P., Polyvinyl alcohol/chitosan wound dressings loaded with antiseptics. *Int. J. Pharm.* **2021**, *593* (120110). https://doi.org/10.1016/j.ijpharm.2020.120110

(19) Kumar, A.; Han, S. S., PVA-based hydrogels for tissue engineering: A review. *Int. J. Polym. Mater. Polym. Biomater.* **2016**, *4037* (June). https://doi.org/10.1080/00914037.2016.1190930

(20) Rivera-Hernandez, G.; Antunes-Ricardo, M.; Martínez-Morales, P.; Sanchez, M., Polyvinyl alcohol based-drug delivery systems for cancer treatment. *Int. J. Pharm.* **2021**, *600* (March), 120478. https://doi.org/10.1016/j.ijpharm.2021.120478

(21) Feldman, D., Poly(vinyl alcohol) recent contributions to engineering and medicine. *J. Compos. Sci.* **2020**, *4* (4), 1–11. https://doi.org/10.3390/jcs4040175

(22) Yang, Q.; Guo, J.; Zhang, S.; Guan, F.; Yu, Y.; Yao, Q.; Zhang, X.; Xu, Y., PVA/PEO/PVA-g-APEG nanofiber membranes with cytocompatibility and anti-cell adhesion for biomedical applications. *Colloids Surfaces A Physicochem. Eng. Asp.* **2023**, *657* (November 2022). https://doi.org/10.1016/j.colsurfa.2022.130638

(23) Mei, Y.; Runjun, S.; Yan, F.; Honghong, W.; Hao, D.; Chengkun, L., Preparation, characterization and kinetics study of chitosan/PVA electrospun nanofiber membranes for the adsorption of dye from water. *J. Polym. Eng.* **2019**, *39* (5), 459–471. https://doi.org/10.1515/polyeng-2018-0275

(24) Januariyasa, I. K.; Ana, I. D.; Yusuf, Y., Nanofibrous poly(vinyl alcohol)/chitosan contained carbonated hydroxyapatite nanoparticles scaffold for bone tissue engineering. *Mater. Sci. Eng. C* **2020**, *107*, 110347. https://doi.org/10.1016/j.msec.2019.110347

(25) Avcu, E.; Baştan, F. E.; Abdullah, H. Z.; Rehman, M. A. U.; Avcu, Y. Y.; Boccaccini, A. R.; Ba, F. E.; Abdullah, H. Z., Electrophoretic deposition of chitosan-based composite coatings for biomedical applications: A review. *Prog. Mater. Sci.* **2019**, *103* (March 2018), 69–108. https://doi.org/10.1016/j.pmatsci.2019.01.001

(26) Liu, B.; Zhang, J.; Guo, H., Research progress of polyvinyl alcohol water-resistant film materials. *Membranes (Basel).* **2022**, *12*, 347. https://doi.org/doi.org/10.3390/membranes12030347

(27) Bistolfi, A.; Massazza, G.; Verné, E.; Massè, A.; Deledda, D.; Ferraris, S.; Miola, M.; Galetto, F.; Crova, M., Antibiotic-loaded cement in orthopedic surgery: A review. *ISRN Orthop.* **2011**, *2011*, 1–8. https://doi.org/10.5402/2011/290851

(28) Haney, V.; Maman, S.; Prozesky, J.; Bezinover, D.; Karamchandani, K., Improving intraoperative administration of surgical antimicrobial prophylaxis: A quality improvement report. *BMJ open Qual.* **2020**, *9* (3), 1–6. https://doi.org/10.1136/bmjoq-2020-001042

(29) Wouthuyzen-Bakker, M.; Löwik, C. A. M.; Knobben, B. A. S.; Zijlstra, W. P.; Ploegmakers, J. J. W.; Mithoe, G.; Al Moujahid, A.; Kampinga, G. A.; Jutte, P. C., Use of gentamicin-impregnated beads or sponges in the treatment of early acute periprosthetic joint infection: A propensity score analysis. *J. Antimicrob. Chemother.* **2018**, *73* (12), 3454–3459. https://doi.org/10.1093/jac/dky354

(30) Vugt van, T. A. G.; Arts, J. J.; Geurts, J. A. P., Antibiotic-loaded polymethylmethacrylate beads and spacers in treatment of orthopedic infections and the role of biofilm formation. *Front. Microbiol.* **2019**, *10* (July), 1–11. https://doi.org/10.3389/fmicb.2019.01626

(31) Metsemakers, W. J.; Fragomen, A. T.; Moriarty, T. F.; Morgenstern, M.; Egol, K. A.; Zalavras, C.; Obremskey, W. T.; Raschke, M.; McNally, M. A., Evidence-based recommendations for local antimicrobial strategies and dead space management in fracture-related infection. *J. Orthop. Trauma* **2020**, *34* (1), 18–29. https://doi.org/10.1097/BOT.0000000000001615

(32) Fang, C.; Wong, T. M.; Lau, T. W.; To, K. K. W.; Wong, S. S. Y.; Leung, F., Infection after fracture

osteosynthesis. Part I: Pathogenesis, diagnosis and classification. *J. Orthop. Surg.* **2017**, *25* (1), 1–13. https://doi.org/10.1177/2309499017692712

(33) Steinmetz, S.; Wernly, D.; Moerenhout, K.; Trampuz, A.; Borens, O., Infection after Fracture Fixation. *EFORT Open Rev.* **2019**, *4* (July), 145–152. https://doi.org/10.1302/2058-5241.4.180093

(34) Tiwari, A.; Sharma, P.; Vishwamitra, B.; Singh, G. Review on surface treatment for implant infection via gentamicin and antibiotic releasing coatings. *Coatings* **2021**, *11* (8). https://doi.org/10.3390/coatings11081006

(35) Thompson, K.; Petkov, S.; Zeiter, S.; Sprecher, C. M.; Geoff Richards, R.; Fintan Moriarty, T.; Eijer, H., Intraoperative loading of calcium phosphate-coated implants with gentamicin prevents experimental *Staphylococcus aureus* infection in vivo. *PLoS One* **2019**, *14* (2). https://doi.org/10.1371/journal.pone.0210402

(36) Teller, M.; Gopp, O.; Neumann, H. G.; Kühn, K. D., Release of gentamicin from bone regenerative materials: An in vitro study. *J. Biomed. Mater. Res. - Part B Appl. Biomater.* **2007**, *81* (1), 23–29. https://doi.org/10.1002/jbm.b.30631

(37) Neut, D.; Dijkstra, R. J. B.; Thompson, J. I.; Kavanagh, C.; Van der Mei, H. C.; Busscher, H. J., A biodegradable gentamicin-hydroxyapatite-coating for infection prophylaxis in cementless hip prostheses. *Eur. Cells Mater.* **2015**, *29*, 42–56. https://doi.org/10.22203/eCM.v029a04

(38) Nichol, T.; Callaghan, J.; Townsend, R.; Stockley, I.; Hatton, P. V.; Le Maitre, C.; Smith, T. J.; Akid, R., The antimicrobial activity and biocompatibility of a controlled gentamicin-releasing single-layer sol-gel coating on hydroxyapatite-coated titanium. *Bone Jt. J.* **2021**, *103 B* (3), 522–529. https://doi.org/10.1302/0301-620X.103B3.BJJ-2020-0347.R1

(39) Tiri, B.; Bruzzone, P.; Priante, G.; Sensi, E.; Costantini, M.; Vernelli, C.; Assunta Martella, L.; Francucci, M.; Andreani, P.; Mariottini, A.; Capotorti, A.; D'Andrea, V.; Francisci, D.; Cirocchi, R.; Cappanera, S., Impact of antimicrobial stewardship interventions on appropriateness of surgical antibiotic prophylaxis: How to improve. *Antibiotics* **2020**, *9* (4). https://doi.org/10.3390/antibiotics9040168

(40) Purba, A. K. R.; Setiawan, D.; Bathoorn, E.; Postma, M. J.; Dik, J. W. H.; Friedrich, A. W., Prevention of surgical site infections: a systematic review of cost analyses in the use of prophylactic antibiotics. *Front. Pharmacol.* **2018**, *9* (Jul). https://doi.org/10.3389/fphar.2018.00776

(41) Rahighi, R.; Panahi, M.; Akhavan, O.; Mansoorianfar, M., Pressure-engineered electrophoretic deposition for gentamicin loading within osteoblast-specific cellulose nanofiber scaffolds. *Mater. Chem. Phys.* **2021**, *272* (May), 125018. https://doi.org/10.1016/j.matchemphys.2021.125018

(42) Stevanović, M.; Djošić, M.; Janković, A.; Kojić, V.; Stojanović, J.; Grujić, S.; Bujagić, I. M.; Rhee, K. Y.; Mišković-Stanković, V., The chitosan-based bioactive composite coating on titanium. *J. Mater. Res. Technol.* **2021**, *15*, 4461–4474. https://doi.org/10.1016/j.jmrt.2021.10.072

(43) Stevanović, M.; Djošić, M.; Janković, A.; Kojić, V.; Vukašinović-Sekulić, M.; Stojanović, J.; Odović, J.; Crevar Sakač, M.; Kyong Yop, R.; Mišković-Stanković, V., Antibacterial graphene-based hydroxyapatite/chitosan coating with gentamicin for potential applications in bone tissue engineering. *J. Biomed. Mater. Res. – Part A* **2020**, 1–15. https://doi.org/10.1002/jbm.a.36974

(44) Stevanović, M.; Djošić, M.; Janković, A.; Nešović, K.; Kojić, V.; Stojanović, J.; Grujić, S.; Matić Bujagić, I.; Rhee, K. Y.; Mišković-Stanković, V., Assessing the bioactivity of gentamicin-preloaded hydroxyapatite/chitosan composite coating on titanium substrate. *ACS Omega* **2020**, *5*, 15433−15445. https://doi.org/10.1021/acsomega.0c01583

(45) Djošić, M.; Janković, A.; Mišković-Stanković, V., Electrophoretic deposition of biocompatible and bioactive hydroxyapatite-based coatings on titanium. *Materials (Basel).* **2021**, *14*, 5391. https://doi.org/https://doi.org/10.3390/ma14185391

(46) Bonetti, L.; Caprioglio, A.; Bono, N.; Altomare, L.; Candiani, G. Mucoadhesive chitosan–methylcellulose oral patches for the treatment of local mouth bacterial infections. *Biomater. Sci.* **2023**,*11*, 2699–2710. https://doi.org/10.1039/d2bm01540d

(47) Rehman, M. A. U.; Batool, S. A. Development of sustainable antibacterial coatings based on electrophoretic deposition of multilayers: gentamicin-loaded chitosan/gelatin/bioactive glass deposition on PEEK/bioactive glass layer. *Int. J. Adv. Manuf. Technol.* **2022**, *120* (5–6), 3885–3900. https://doi.org/10.1007/s00170-022-09024-3

(48) Aydemir, T.; Pastore, J. I.; Jimenez-Pique, E.; Roa, J. J.; Boccaccini, A. R.; Ballarre, J. Morphological and mechanical characterization of chitosan/gelatin/silica-gentamicin/bioactive glass coatings on orthopaedic metallic implant materials. *Thin Solid Films* **2021**, *732* (May), 138780. https://doi.org/10.1016/j.tsf.2021.138780

(49) Stevanović, M.; Đošić, M.; Janković, A.; Kojić, V.; Vukašinović-Sekulić, M.; Stojanović, J.; Odović, J.; Crevar Sakač, M.; Rhee, K. Y.; Mišković-Stanković, V., Gentamicin-loaded bioactive hydroxyapatite/chitosan composite coating electrodeposited on titanium. *ACS Biomater. Sci. Eng.* **2018**, *4* (12), 3994–4007. https://doi.org/10.1021/acsbiomaterials.8b00859

(50) Aydemir, T.; Liverani, L.; Pastore, J. I.; Ceré, S. M.; Goldmann, W. H.; Boccaccini, A. R.; Ballarre, J., Functional behavior of chitosan/gelatin/silica-gentamicin coatings by electrophoretic deposition on surgical grade stainless steel. *Mater. Sci. Eng. C* **2020**, *115*, 111062. https://doi.org/10.1016/j.msec.2020.111062

(51) Djošić, M.; Janković, A.; Stevanović, M.; Stojanović, J.; Vukašinović-Sekulić, M.; Kojić, V.; Mišković-Stanković, V., Hydroxyapatite/poly(vinyl alcohol)/chitosan coating with gentamicin for orthopedic implants. *Mater. Chem. Phys.* **2023**, *303*, 127766. https://doi.org/10.1016/j.matchemphys.2023.127766

(52) Murdan, S.; Kerai, L.; Hossin, B., To what extent do in vitro tests correctly predict the in vivo residence of nail lacquers on the nail plate? *J. Drug Deliv. Sci. Technol.* **2015**, *25* (February), 23–28. https://doi.org/10.1016/j.jddst.2014.11.002

(53) Duta, L.; Popescu, A. C., Current status on pulsed laser deposition of coatings from animal-origin calcium phosphate sources. *Coatings* **2019**, *9*, 335. https://doi.org/10.3390/coatings9050335

(54) Igeta, K.; Kuwamura, Y.; Horiuchi, N.; Nozaki, K.; Shiraishi, D.; Aizawa, M.; Hashimoto, K.; Yamashita, K.; Nagai, A., Morphological and functional changes in RAW264 macrophage-like cells in response to a hydrated layer of carbonate-substituted hydroxyapatite. *J. Biomed. Mater. Res. Part A* **2017**, *105*, 1063–1070. https://doi.org/10.1111/pce.14045

(55) Pishbin, F.; Mouriño, V.; Flor, S.; Kreppel, S.; Salih, V.; Ryan, M. P.; Boccaccini, A. R., Electrophoretic deposition of gentamicin-loaded bioactive glass/ chitosan composite coatings for orthopaedic implants. *ACS Appl. Mater. Interfaces* **2014**, *6* (11), 8796–8806. https://doi.org/10.1021/am5014166

(56) Guo, X.; Wu, Y.; Yan, N., In situ micro-FTIR observation of molecular association of adsorbed water with heat-treated wood. *Wood Sci. Technol.* **2018**, *52* (4), 971–985. https://doi.org/10.1007/s00226-018-1020-3

(57) Ren, F.; Ding, Y.; Leng, Y., Infrared spectroscopic characterization of carbonated apatite: A combined experimental and computational study. *J. Biomed. Mater. Res. – Part A* **2014**, *102* (2), 496–505. https://doi.org/10.1002/jbm.a.34720

(58) Solodyankina, A.; Nikolaev, A.; Frank-Kamenetskaya, O.; Golovanova, O., Synthesis and characterization of nanocrystalline apatites from solution modeling human blood. *J. Mol. Struct.* **2016**, *1119*, 484–489. https://doi.org/10.1016/j.molstruc.2016.04.080

(59) Barinov, S. M.; Rau, J. V.; Cesaro, S. N.; Ďurišin, J.; Fadeeva, I. V.; Ferro, D.; Medvecky, L.; Trionfetti, G., Carbonate release from carbonated hydroxyapatite in the wide temperature rage. *J. Mater. Sci. Mater. Med.* **2006**, *17* (7), 597–604. https://doi.org/10.1007/s10856-006-9221-y

(60) Djošić, M. S.; Mitrić, M.; Mišković-Stanković, V. B., The porosity and roughness of electrodeposited calcium phosphate coatings in simulated body fluid. *J. Serb. Chem. Soc.* **2015**, *80* (2), 237–251. https://doi.org/10.2298/JSC140626098D

(61) Shi, Y. Y.; Li, M.; Liu, Q.; Jia, Z. J.; Xu, X. C.; Cheng, Y.; Zheng, Y. F., Electrophoretic deposition of graphene oxide reinforced chitosan–hydroxyapatite nanocomposite coatings on Ti substrate. *J. Mater. Sci. Mater. Med.* **2016**, *27* (3), 1–13. https://doi.org/10.1007/s10856-015-5634-9

(62) Macha, I. J.; Cazalbou, S.; Ben-Nissan, B.; Harvey, K. L.; Milthorpe, B., Marine structure derived calcium phosphate-polymer biocomposites for local antibiotic delivery. *Mar. Drugs* **2015**, *13* (1), 666–680. https://doi.org/10.3390/md13010666

(63) Kamaly, N.; Yameen, B.; Wu, J.; Farokhzad, O. C., Nanoparticles: mechanisms of controlling drug release. *Chem Rev.* **2016**, *116* (4), 2602–2663. https://doi.org/10.1021/acs.chemrev.5b00346.Degradable

(64) Bhattacharjee, B. N.; Mishra, V. K.; Rai, S. B.; Parkash, O.; Kumar, D., Structure of apatite nanoparticles derived from marine animal (crab) shells: An environment-friendly and cost-effective novel approach to recycle seafood waste. *ACS Omega* **2019**, *4* (7), 12753–12758. https://doi.org/10.1021/acsomega.9b00134

(65) Madupalli, H.; Pavan, B.; Tecklenburg, M. M. J., Carbonate substitution in the mineral component of bone: discriminating the structural changes, simultaneously imposed by carbonate in A and B sites of apatite. *J. Solid State Chem.* **2017**, *255* (May), 27–35. https://doi.org/10.1016/j.jssc.2017.07.025

(66) Ritger, P. L.; Peppas, N. A., A Simple equation for description of solute release II. Fickian and anomalous release from swellable devices. *J. Control. Release* **1987**, *5* (1), 37–42. https://doi.org/10.1016/0168-3659(87)90035-6

(67) Papich, M., Antibiotic drug selection for equine bacterial pathogens. *Saunders Handb. Vet. Drugs* **2016**, 874. https://doi.org/10.1016/b978-0-323-24485-5.00041-3

(68) Pankey, G. A.; Sabath, L. D., Clinical relevance of bacteriostatic versus bactericidal mechanisms of action in the treatment of gram positive bacterial infections. *Clin. Infect. Dis.* **2004**, *38* (6), 864–870. https://doi.org/10.1086/381972